scientific reports

Check for updates

OPEN

Research on permanent magnet synchronous motor algorithm based on linear nonlinear switching self-disturbance rejection control

Xiangde Liu[1], Yu Li[1,2], Liang Xia[2]✉, Xianfeng Tan[2] & Xiang Cao[2]

This paper presents a linear-nonlinear switching control strategy, called Switching Active Disturbance Rejection Control (SADRC), to enhance the disturbance rejection capability of the speed controller in a servo system. SADRC combines the advantages of Linear Active Disturbance Rejection Control (LADRC) and Nonlinear Active Disturbance Rejection Control (NLADRC), and introduces a parameter to switch between nonlinear and linear control, thereby improving the robustness of the servo system. Firstly, the mathematical model of the motor is analyzed as the starting point of the paper. Then, the basic principles of Active Disturbance Rejection Control (ADRC) are analyzed, and improvements are made to address its limitations, resulting in the design of SADRC. The parameters introduced in SADRC are analyzed to determine their appropriate ranges. Finally, the performance of SADRC is validated by comparing the rotational effects of Permanent Magnet Synchronous Motor (PMSM).

It is well known that the servo system takes the difference between the set value and the feedback value as input. The servo system is commonly used in fields such as industrial robotic arms, aerospace, and CNC machine tools, which require high motor performance and control accuracy[1,2]. Taking industrial robotic arms as an example, the control performance of the servo system directly determines the production speed and product quality of the production line. Therefore, improving the robustness of the servo system is of great significance. The overall performance of the servo system is mainly determined by two parts. One is the hardware aspect, such as the operating speed and control frequency of the control chip, the accuracy of the encoder, the motor structure[3–5], and the motor type[6]. The other aspect is the control algorithm, and different control algorithms also determine the performance of the entire system. Among them, the speed controller and current controller commonly use PI control. Due to its simplicity and good performance, PI control is widely used in the industrial control field. However, with the continuous improvement of industrial requirements, ordinary PI control is difficult to meet the requirements of high-performance servo systems. It is of great significance to improve the robustness of the servo system through optimized control algorithms. Many scholars have conducted in-depth research on control algorithms, such as proportional-integral (PI) control with feedforward compensation, disturbance-based control[7], Sliding Mode Control (SMC)[8–10], Model Predictive Direct Speed Control (MP-DSC) [11] and Active Disturbance Rejection Control (ADRC), etc.

ADRC was initially proposed by researcher Han[12]. It is a nonlinear structure created by combining modern control theory with the PID controller. Subsequently, through the efforts of scholars such as Gao Zhiqiang, the bandwidth method was used to solve the parameter tuning and linearization issues of ADRC, enabling its application in engineering practice[13,14]. However, Linear Active Disturbance Rejection Control (LADRC) has a constant gain, which leads to large initial state errors and delayed response speed. In comparison, Nonlinear Active Disturbance Rejection Control (NLADRC) has higher tracking accuracy, stronger disturbance rejection capability, and faster response. However, the stability and reliability analysis of NLADRC is extremely difficult, which greatly hinders the practical application of ADRC[15,16]. Therefore, how to further enhance the robustness of the ADRC controller remains a challenge. In this regard, some scholars have conducted further research based on the ADRC framework. For example, Li et al. used the ADRC algorithm with an Extended State Observer (ESO) to suppress disturbances in control systems[17]. Qi provided proof of stability for NLADRC[18,19]. Zhao demonstrated the convergence of nonlinear active disturbance rejection, providing theoretical support for its application[20]. On the other hand, combining the advantages of LADRC and NLADRC can greatly improve

[1]Chongqing University of Posts and Telecommunications, Chongqing 400065, China. [2]Chongqing Robotics Institute, Chongqing 400000, China. ✉email: 112182504@qq.com

system performance. Hao directly selected LADRC and NLADRC based on the magnitude of the system input error. Although this approach is simple to operate, it involves complex calculations, especially during controller switching moments[21]. Lin designed the ESO module, but the constructed function had discontinuous states[22]. In this paper, we construct the ESO module, add parameters, and achieve a smooth transition from nonlinear to linear by designing a Switching Active Disturbance Rejection Control (SADRC) that combines the advantages of LADRC and NLADRC. Finally, the performance of SADRC is validated through comparative experimental data on Permanent Magnet Synchronous Motor (PMSM).

Mathematical model of permanent magnet synchronous motor

The object of control in this study is the permanent magnet synchronous motor. Assuming that the windings are symmetrical and disregarding core saturation, eddy current loss, and hysteresis loss, the mathematical model of a PMSM can be derived based on motor control theory. The stator-side voltage equation is shown in the following Eq. (1).

$$\begin{cases} u_d = R_s i_d + \frac{d\psi_d}{dt} - \omega\psi_q \\ u_q = R_s i_q + \frac{d\psi_q}{dt} - \omega\psi_d \end{cases} \tag{1}$$

where u_d, u_q is the stator voltage component of the d-q coordinate system, ψ_d ψ_q is the stator flux component, and ω is the rotational angular velocity. The flux equation is (2).

$$\begin{cases} \psi_q = L_q i_q \\ \psi_d = L_d i_d + \psi_f \end{cases} \tag{2}$$

where L_d, L_q is the inductance component of the d and q axes, and ψ_f is the permanent magnet flux linkage.

This can be obtained from the above formula:

$$\begin{cases} u_d = R_s i_d + L_d \frac{di_d}{dt} - \omega_r L_{qq} i_q \\ u_q = R_s i_q + L_q \frac{di_q}{dt} + \omega_r L_d i_d + \omega_r \psi_f \end{cases} \tag{3}$$

Electromagnetic torque equation for PMSM:

$$T_e = \frac{3}{2} P_n \left[\psi_f i_q + \left(L_d - L_q \right) i_d i_q \right] \tag{4}$$

Among them T_e is electromagnetic torque; P_n is the number of pole pairs, and other parameters are the same as above. Mechanical equations of motion for PMSM:

$$T_e - T_l = J \frac{dw_r}{dt} \tag{5}$$

where T_l is the load torque; J is the moment of inertia.

ADRC control principle

LADRC control principle

ADRC is mainly composed of three parts: the tracking differentiator, the extended state observer, and the state error feedback control rate. The core idea of self-disturbance rejection control is to proactively extract disturbance information from the input/output signal of the controlled object before it significantly affects the final output of the system. This information is then used to eliminate the disturbance as quickly as possible using the control signal, thereby minimizing its impact on the controlled quantity.

The control object in this paper is a first-order system, specifically a permanent magnet synchronous motor. This type of motor is primarily utilized in the field of industrial robotic arms. The following state-space equation can be obtained. This is shown in the following Eq. (6).

$$\begin{cases} \dot{x_1} = x_2 + bu \\ \dot{x_2} = f(x_1, x_2) \end{cases} \tag{6}$$

The lower x_1 is the system variable, $f(x_1, x_2)$ is the total disturbance of the system, b is the estimate of the gain of the control system, and u is the system input variable. The permanent magnet synchronous motor adopts a double closed-loop vector control system. The current loop utilizes traditional PI control, while the speed loop utilizes the SADRC. The control system is an inertial system. It takes a certain amount of time for the speed to reach the desired speed from zero. At the initial moment, there is a significant difference between the desired speed and the velocity feedback, resulting in a large overshoot. To achieve this, the transition process is designed to gradually increase the velocity. The equation for this process is as follows:

$$\begin{cases} \dot{v}_1 = v_2 \\ \dot{v}_2 = -r^2(v_1 - v_0(t)) - 2rv_2 \end{cases} \tag{7}$$

$v_0(t)$ represents the given speed and r is the speed factor. v_1 is the tracking value of $v_0(t)$, v_2 is the derivative of v_1 and r is the speed factor. ESO is a vital part of ADRC for real-time estimation of system variables, real-time

estimation and compensation of total disturbances, elimination of disturbances, and improved control. For first-order systems, LESO can be designed as follows:

$$\begin{cases} e = z_1 - v_f \\ \dot{z}_1 = z_2 - \beta_1' e + b_0 u \\ \dot{z}_2 = -\beta_2' e \end{cases} \tag{8}$$

where z_1, z_2 are the state variables of the observer, z_1 are used to track v_1, z_2 is the estimation of the total perturbation, β_1', β_2' are the gain factors of z_1, and z_2, respectively, and e is the error between the estimated value and the output value. The output of LESO is as follows:

$$u = \frac{u_0 - z_2}{b_0} \tag{9}$$

In a first-order linear system, LSEF can design P control:

$$u_0 = K_1(v_1 - z_1) \tag{10}$$

where K_1 are the gain factors of the error.

NLADRC control principle

The first-order NLADRC transition process is improved on LADRC:

$$\begin{cases} \dot{v}_1 = v_2 \\ \dot{v}_2 = \text{fhan}\,(v_1 - v_0(t), v_2, r, h) \end{cases} \tag{11}$$

h is the step size. "fhan" is the fastest tracking function, as follows:

$$\begin{cases} d = rh^2, a_0 = hx_2, y = x_1 + a_0, a_1 = \sqrt{d\left(d + 8\left|y\right|\right)} \\ a_2 = a_0 + sign(y)(a_1 - d)/2 \\ a_3 = (sign(y + d) - sign(y - d))/2 \\ a_4 = \left(a_0 + y - a_2\right)a_3 + a_2 \\ a_5 = \left(sign(a_4 + d) - sign(a_4 - d)\right)/2 \\ \text{fhan}\,(x_1, x_2, r, h) = -r\left(\frac{a_4}{d} - sign(a_4)\right)a_5 - rsign(a_4) \end{cases} \tag{12}$$

The transition process of NLADRC and LADRC is similar, and f can be replaced with the "fhan" function. NLESO introduces the nonlinear function $fal(e, \alpha_i, \delta)$, which makes the observer have the characteristics of "small error, large gain, large error, small gain", the specific expression is as follows:

$$\begin{cases} e = z_1 - y \\ \dot{z}_1 = z_2 - \beta_1 fal(e, \alpha_1, \delta) + b_0 u \\ \dot{z}_2 = -\beta_2 fal(e, \alpha_1, \delta) \end{cases} \tag{13}$$

where the expression for the nonlinear function $fal(e, \alpha_i, \delta)$ is:

$$fal(e, \alpha_i, \delta) = \begin{cases} \frac{e}{\delta^{1-\alpha_i}} & |e| \le \delta \\ |e|^{\alpha_i} sign(e) & |e| > \delta \end{cases} \tag{14}$$

where β_1, β_2 is the gain factor, α_1, α_2, and δ are pending parameters. The nonlinear state error feedback rate is also introduced into the nonlinear $fal(e, \alpha_i, \delta)$ function as follows:

$$u_0 = k_1 \text{ fal}\left(v_1 - z_1, \alpha_1', \delta'\right) \tag{15}$$

Among them, k_1 is tunable parameters, and α_1' and δ' are the two pending parameters of NLSEF.

SADRC design

LADRC and NLADRC have their own advantages. LADRC is characterized by easy parameter adjustment and easy implementation in engineering. It is particularly effective when the error is large, as it allows for a large control gain. NLADRC has the characteristics of "small error, large gain, large error, small gain". In other words, NLADRC has a stronger adjustment ability when the error is small. As a switch, SADRC switches to NLADRC when the error is small and LADRC when the error is large, effectively utilizing the benefits of both LADRC and NLADRC. The framework of SADRC is shown in Fig. 1, v_f the speed is given, and the speed step increases uniformly in the TD part. SESO is a system expansion state observer used to detect system state variables in real time. SSEF is the state error feedback rate, the input error signal is processed, the output u_0 is different from the compensation value of the observer. Finally, it is input into the control system.

In the TD section, there is no clear distinction between LADRC and NLADRC, and there is no need to create a separate toggle switch. In the experiment, the discrete form of the TD part is designed as follows.

$$\begin{cases} f = -r^2\left(v_1 - v_f\right) - 2rv_2 \\ v_1 = v_1 + v_2 h \\ v_2 = v_2 + fh \end{cases} \tag{16}$$

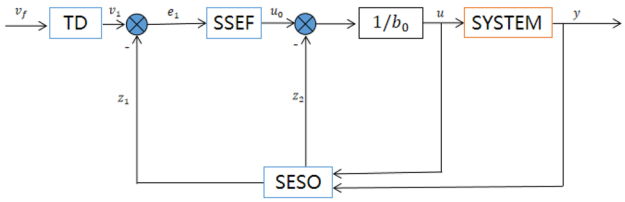

Figure 1. SADRC flow block diagram.

where f and v_2 are intermediate variables, and v_f is given velocity.

Design of SESO and SSEF

The core of SADRC lies in the design of the $fal_s(e, \alpha_i, \delta_1, \delta_2)$ function in SESO, which not only needs to meet the good control effect of NLADRC in the case of "small error", but also requires LADRC to have a large gain when the error is large. Figure 2 is the function curve of $fal(e, \alpha_i, \delta)$.

It can be seen from the curve that the smaller the value of the α_i, the stronger the nonlinearity of the $fal(e, \alpha_i, \delta)$ function. Additionally, there is a greater the gain in the case of small errors, but the increase in gain is slower for large errors. In addition, δ is the critical point of the linear interval of $fal(e, \alpha_i, \delta)$, the smaller the δ, the smaller the linear interval of the $fal(e, \alpha_i, \delta)$ function, the stronger the nonlinearity. In NLADRC, generally through continuous debugging α_i, δ two parameters make the control effect of the system moderate, but it is impossible to ensure that the system can maintain a high control effect when the error changes in a large range. Therefore, this paper designs a class of function curves that maintain high gain and fast response speed even if the error fluctuates in a wide range, and the $fal_s(e, \alpha_i, \delta_1, \delta_2)$ function is designed as follows:

$$fal_s(e, \alpha_i, \delta_1, \delta_2) = \begin{cases} e\delta_1^{\alpha_i - 1} & |e| \le \delta_1 \\ |e|^{\alpha_i} sign(e) & \delta_1 < |e| < \delta_2 \\ K_c e\delta_2^{\alpha_i - 1} & |e| \ge \delta_2 \end{cases} \tag{17}$$

Among them, in order to ensure the system performance, the K_c generally takes a value of 1, which can be adjusted according to the needs of the system. $fal_s(e, \alpha_i, \delta_1, \delta_2)$ function compared with the $fal(e, \alpha_i, \delta)$ function, the introduction of δ_2, δ_2 changes the gain of the controller under large error conditions, that is, the advantages of LADRC in large error conditions are fused. An image of the $fal_s(e, \alpha_i, \delta_1, \delta_2)$ function is shown below. It can be seen from the curve that when the error range is $-\delta_1 < e < \delta_1$, SADRC presents nonlinear characteristics, when the error range is $|e| \ge \delta_2$, SADRC has the properties of LADRC, $fal_s(e, \alpha_i, \delta_1, \delta_2)$ function combines the advantages of LADRC and NLADRC. The effect of δ_2 on the system is shown in Fig. 3.

In this experiment, SADRC is applied to the servo-controlled speed loop, so the system output y is the speed feedback v_f, then SESO can be designed:

$$\begin{cases} e = z_1 - v_f \\ \dot{z}_1 = z_2 - \beta_1 fal_s(e, \alpha_1, \delta_1, \delta_2) + b_0 u \\ \dot{z}_2 = -\beta_2 fal_s(e, \alpha_2, \delta_1, \delta_2) \end{cases} \tag{18}$$

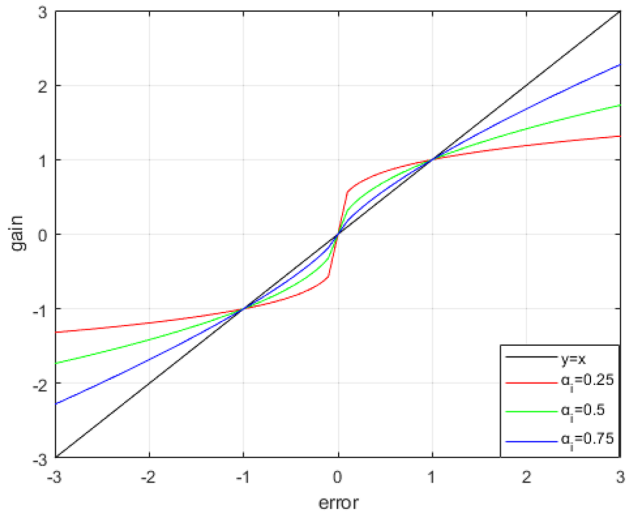

Figure 2. $fal(e, \alpha_i, \delta)$ function curve.

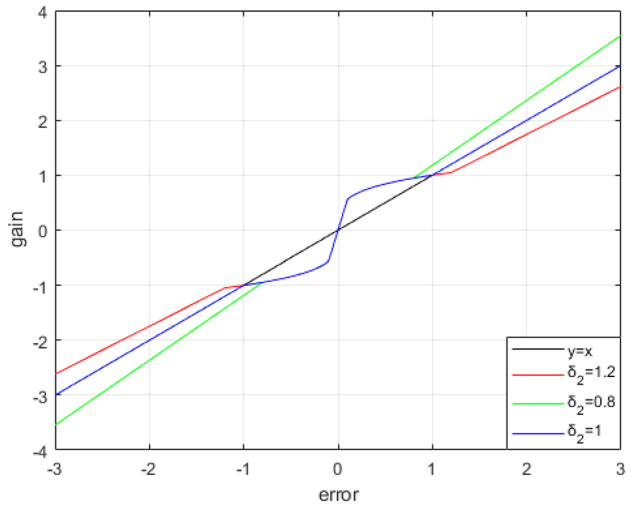

Figure 3. $fal_s(e, \alpha_i, \delta_1, \delta_2)$ curves.

where z_1 is the state variable given by the tracking speed, z_2 is the system interference value, β_1, β_2 are the coefficients to be determined, and u is the system output, as follows:

$$u = \frac{u_0 - z_2}{b_0} \tag{19}$$

u_0 is the output of SSEF, this experiment uses first-order SADRC, so SSEF directly uses proportional control, and SSEF is designed as:

$$u_0 = k_p fal_s\left(e, \alpha_1{}', \delta_1{}', \delta_2{}'\right) \tag{20}$$

SADRC parameter tuning

SESO

The extended state observer is the core of the disturbance rejection control, which observes and compensates for the system disturbance in real time. The parameters to be determined are: $\beta_1, \beta_2, \alpha_1, \alpha_2, \delta_1, \delta_2$. β_1, β_2 can be adjusted according to the bandwidth method. In order to ensure system stability the range of $\alpha_1, \alpha_2, \delta_1, \delta_2$ can be reduced to: $0 < \alpha_1 < \alpha_2 < 1, 0 < \delta_1 < \delta_2 \leq 1$, the specific parameter setting process is as follows.

(18) is obtained by performing the Laplace transform:

$$\begin{cases} e = z_1 - v_f \\ \mathrm{sz}_1 = z_2 - \beta_1 fal_s(e, \alpha_1, \delta_1, \delta_2) + b_0 u \\ \mathrm{sz}_2 = -\beta_2 fal_s(e, \alpha_2, \delta_1, \delta_2) \end{cases} \tag{21}$$

The bandwidth method for parameter tuning reference, let $fal_s(e, \alpha_1, \delta_1, \delta_2) = \lambda_1(e)e$, $al_s(e, \alpha_2, \delta_1, \delta_2) = \lambda_2(e)e$, (21) can be written as:

$$\begin{cases} e = z_1 - v_f \\ \mathrm{sz}_1 = z_2 - \beta_1 \lambda_1(e)e + b_0 u \\ \mathrm{sz}_2 = -\beta_2 \lambda_2(e)e \end{cases} \tag{22}$$

From (22), we get the following transfer function model:

$$z_1 = \frac{\beta_1 \lambda_1(e) v_f s + \beta_2 \lambda_2(e) v_f + b_0 us}{s^2 + \beta_1 \lambda_1(e) s + \beta_2 \lambda_2(e)} \tag{23}$$

$$z_2 = \frac{\beta_2 \lambda_2(e) s v_f - \beta_2 \lambda_2(e) b_0 u}{s^2 + \beta_1 \lambda_1(e) s + \beta_2 \lambda_2(e)} \tag{24}$$

Parameter tuning of reference[16], $\beta_1 = 3w_0$, $\beta_2 = 0.6w_0^2$, SESO has a good suppression effect on the system output, and the influence of u can be ignored for analysis.

$$\frac{z_1}{v_f} = \frac{3w_0 s + 0.6w_0^2}{s^2 + 3w_0 s + 0.6w_0^2} \tag{25}$$

The frequency domain characteristic analysis plot of the system can be obtained from the transfer function, and it can be seen from the Fig. 4, with the increase of w_0, the dynamic performance of SADRC is better. But in actual operation, the increase in w_0 also makes the motor control effect more ideal, too large w_0 will cause motor shaking and motor noise. Therefore, in the process of parameter adjustment, the w_0 should be gradually increased from a small value, and the w_0 when the motor is shaken is its critical value. that the smaller the α_i, the stronger the nonlinearity of SADRC, but too small α_i will cause the motor to produce high-frequency oscillation, in this experiment, 0.25 and 0.5 were taken α_1 and α_2, respectively δ_1 and δ_2 determine the size of the nonlinear interval of SADRC, According to the system requirements, δ_1 and δ_2 are 0.05 and 1 respectively.

TD

There are two adjustable parameters in this expression, step h and speed factor r. Step h is set to 0.01s, when the motor from the prohibition to the rated speed, the curve of different speed coefficients r is shown in Fig. 5, where the black line is the speed given, the red line is the speed given through the transition process of the speed output

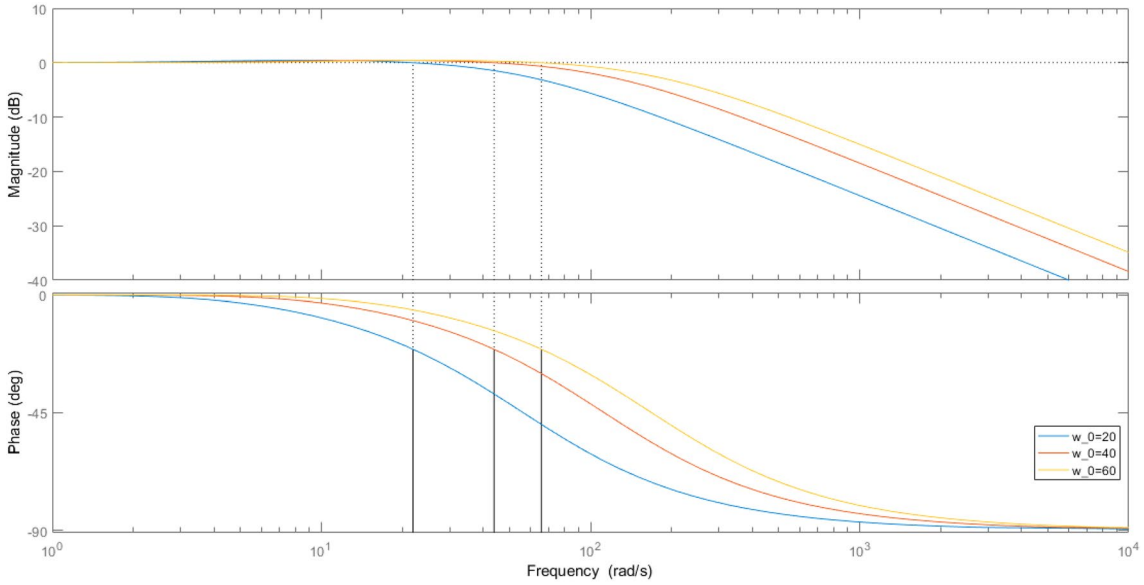

Figure 4. Bode plot of the transfer function.

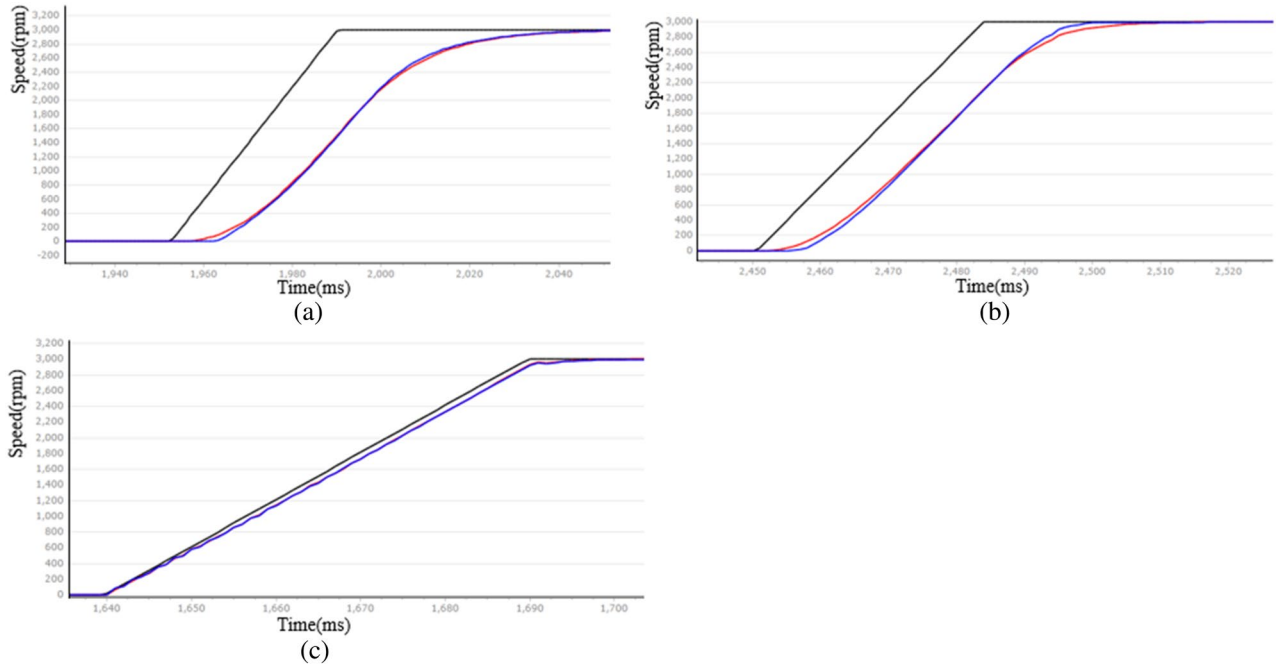

Figure 5. r velocity curve corresponding to different values (**a**) r = 5, (**b**) r = 10, (**c**) r = 200.

v_1, and the blue line is the speed feedback. The abscissa represents time, 4ms/scale, and the ordinate represents speed (the following coordinate diagrams are based on this standard).

This can be seen from Fig. 5, when r is 5 and 10, the rise time is 344ms and 192ms (sampled every 4ms), respectively, and when r increases to 200, the v_1 almost coincides with the given speed. Therefore, with the increase of r, the motor can reach the rated speed faster, but too large r will make the transition process invalid. In this experiment, $r = 200$ and $h = 0.01$ were taken.

SSEF

Introduce $fal_s(e, \alpha_i, \delta_1, \delta_2)$ into the SEF, named SSEF. The state error feedback control rate is shown in Eq. (20), directly using proportional control, the pending parameters are: $k_p, \alpha_1\prime, \delta_1\prime, \delta_2\prime, b_0$ where $\alpha_1\prime, \delta_1\prime, \delta_2\prime$ are similar to the three parameters in SESO, and only need to be fine-tuned. In general, $\delta_1\prime$ should be within the interval [0.01, 0.1]. Therefore, in this experiment $\alpha_1\prime$, $\delta_1\prime$ and $\delta_2\prime$ are taken as 0.5, 0.1, and 1, respectively. b_0 determines the robustness of the system, the larger the b_0, the more stable the system, but the control effect is relatively poor. k_p is similar to PD-controlled k_1, and the b_0 and k_p of this experiment are taken as 20 and 380, respectively.

Experimental results and analysis

Experimental platform

In order to evaluate the performance of SADRC, this paper conducts experiments on the following platform and compares the experimental data with that of LADRC and NLADRC. In this paper, the selected experimental motor is a 400W surface-mounted permanent magnet synchronous motor with a holding gate line. In both the step experiment and the steady-state experiment, the motor is in the under-load state with a load size of 1 kg, as shown in Fig. 6. Since position information is not required for the experiment, the speed-current double closed-loop mode is used. The absolute encoder monitors and provides real-time feedback on the motor speed. The surface-mount permanent magnet synchronous motor is a hidden-pole motor with a $i_d = 0$ control strategy that ensures a linear relationship between the Q-axis current and the output torque. Table 1 provides a comprehensive list of parameters for PMSM.

In this experiment, SADRC is applied to a servo-controlled speed loop, while the current loop is controlled by PI controller and the motor rotation is controlled by Field-Oriented Control (FOC). Closed-loop control is

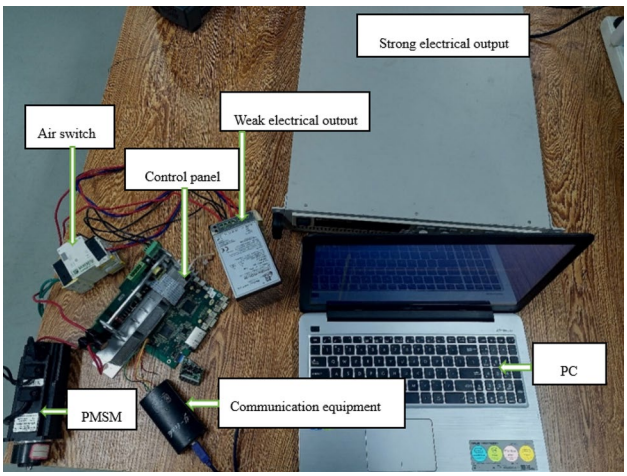

Figure 6. Experimental platform.

Power (P)	400 W
Inertia (J)	0.315×10^{-4} kg m^2
D-axis inductance (L_d)	5.553 mH
Q-axis inductance (L_q)	5.553 mH
Number of pole pairs (P_n)	5
Rated speed (n)	3000 rpm
Rated current (I)	2.9 A
Back electromotive-force constant	18.25 V/Krpm
Resistance	1.544 Ω

Table 1. List of PMSM parameters.

achieved by acquiring current information through the use of a sampling resistor. Finally, the experiment uses a PWM carrier frequency of 5kHz, and the specific control block diagram is shown in Fig. 7.

The rated speed of the motor is 3000 rpm, and the high current module can provide a voltage of 310V. The MCU adopts the STM32F407 chip, which has a maximum frequency of 168MHz. This frequency is sufficient to meet the control frequency requirements of the LADRC, NLADRC, and SADRC. The air switch is responsible for circuit protection, while the upper computer is responsible for algorithm parameter adjustment, data collection, and data collation.

Step experiments

The essence of the industrial robotic arm's action lies in the rotation of the PMSM. The speed curve of the PMSM is analyzed at two given speeds: 1000 rpm and 3000 rpm. The black line represents the given speed curve, while the red line represents the speed feedback curve. This is shown in Figs. 8 and Fig. 9. Figure 10 shows the PMSM velocity decline phase curve. The horizontal axis of the following graph represents time, with a specific scale of 4 ms/1.

Therefore, the LADRC control has a positive impact on the speed rise and fall stages, but it experiences a delay during the initial start and results in significant overshoot. NLADRC deviates from the speed given curve in the rising and falling stages of the velocity feedback curve, and this deviation increases. This is due to the nonlinear function characteristics of NLADRC. As the error increases, the gain of NLADRC increases at a slower rate, which results in minimal overshoot in NLADRC speed feedback. SADRC has obvious advantages in terms of response time, overshoot, and adjustment time, and the specific data are shown in Table 2 (Supplementary Information).

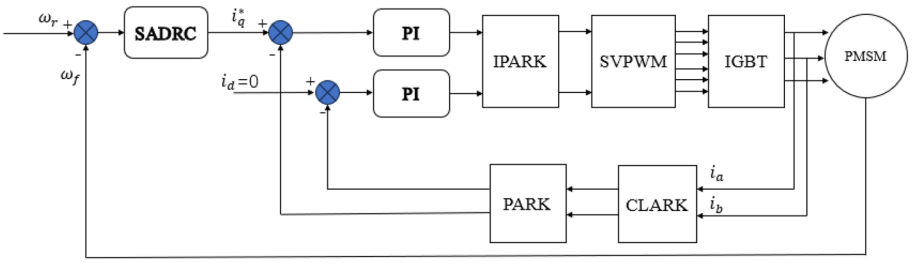

Figure 7. Servo control block diagram based on SADRC.

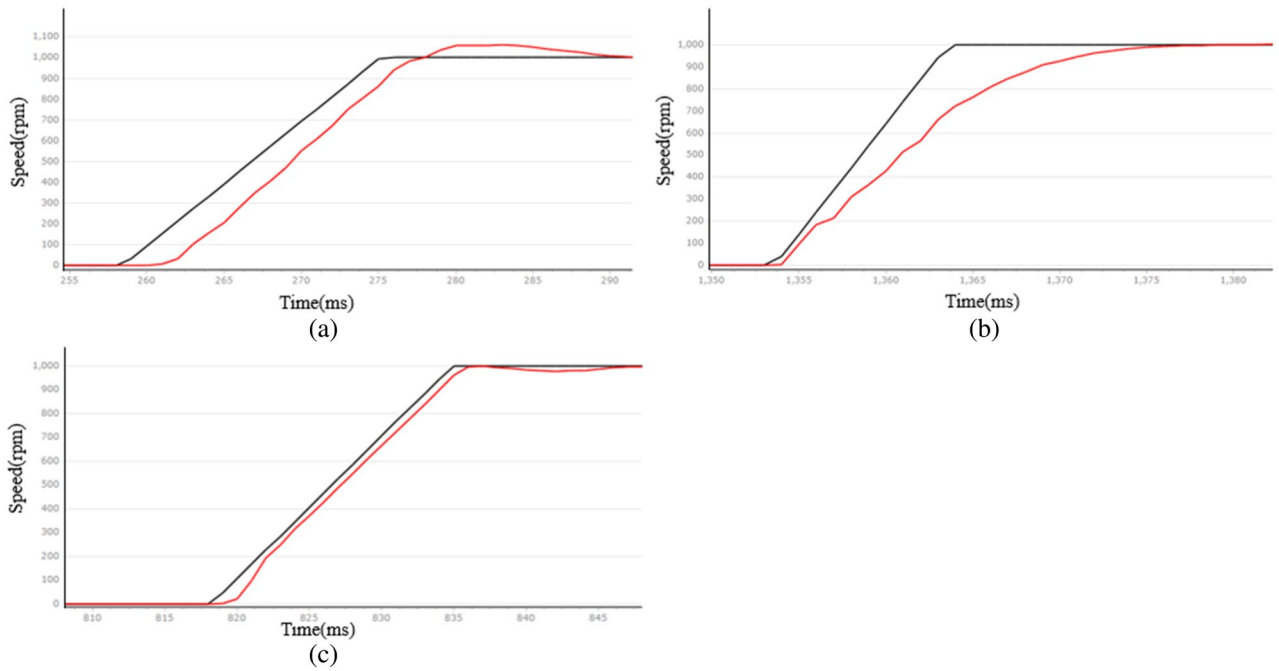

Figure 8. PMSM velocity rise curve at 1000 rpm given speed (**a**) LADRC, (**b**) NLADRC, (**c**) SADRC.

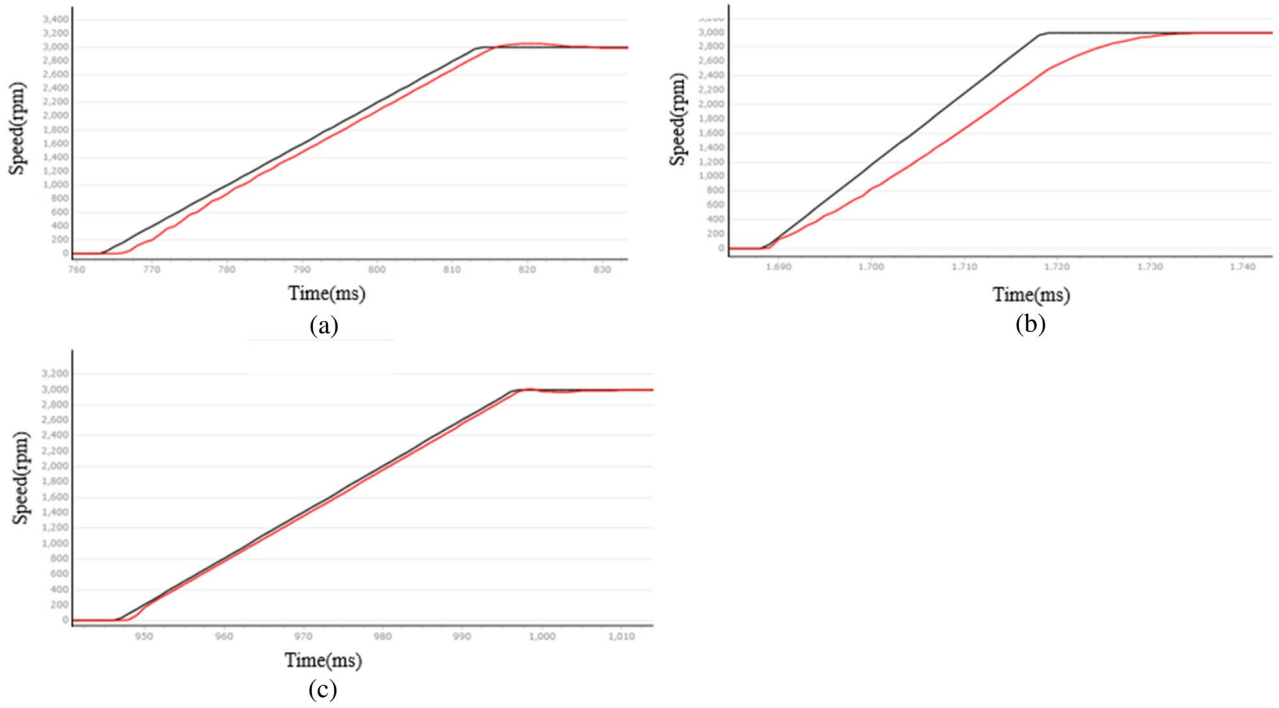

Figure 9. PMSM velocity rise curve at 3000 rpm given speed (**a**) LADRC, (**b**) NLADRC, (**c**) SADRC.

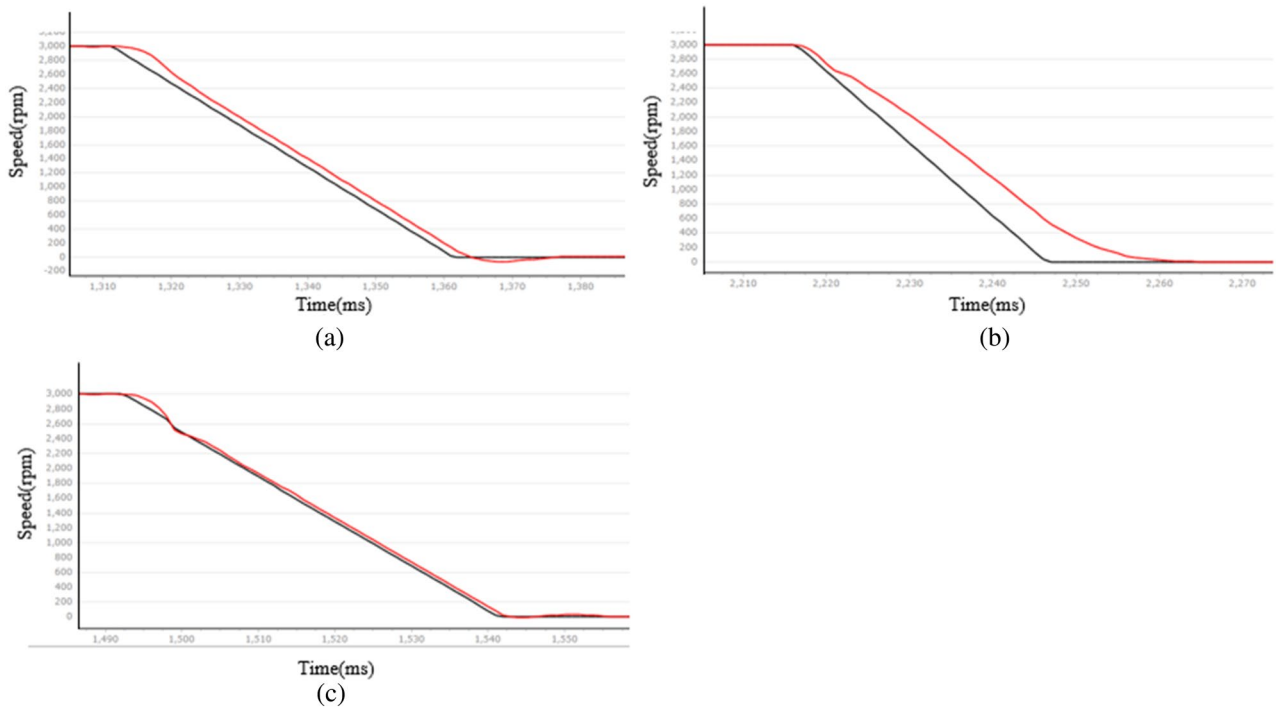

Figure 10. PMSM velocity decline curve at a given speed of 3000 rpm (**a**) LADRC, (**b**) NLADRC, (**c**) SADRC.

Steady-state performance

The overall stability of the industrial robotic arm is determined by the steady-state performance of the motor. This paper compares the steady-state error of the speed curve of three control algorithms to reflect the steady-state performance, as shown in Fig. 11.

NLADRC is nonlinear and prone to high-frequency oscillations when the speed reaches a steady state. High-frequency oscillations can be attenuated by adjusting the corresponding parameters, but this may also lead to a deterioration in the control effect. Table 3 displays the average steady-state error for the three controllers.

Target rotational speed v_f (rpm)	Control algorithms	Overshoot σ (rpm)	Adjust the time t_s (ms)
1000	LADRC	58	220
	NLADRC	4	112
	SADRC	2	72
3000	LADRC	62	344
	NLADRC	5	216
	SADRC	5	192

Table 2. Comparison of PMSM start-stop performance.

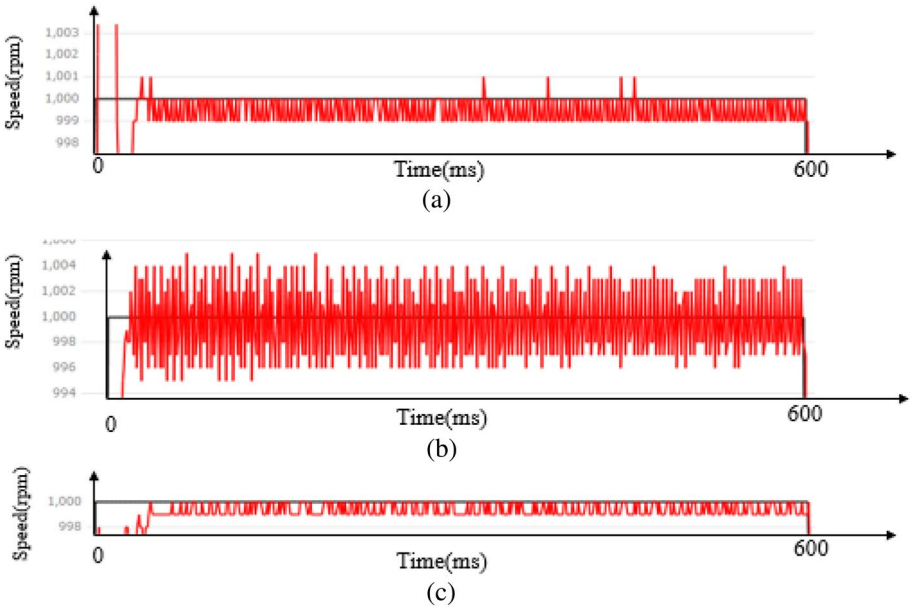

Figure 11. Steady-state curve of PMSM at a given speed of 1000 rpm (**a**) LADRC, (**b**) NLADRC, (**c**) SADRC.

	LADRC	NLADRC	SADRC
$\frac{\sum_1^n \lvert e \rvert}{n}$	0.72	1.89	0.66

Table 3. Comparison of PMSM steady-state errors.

Load mutation experiments

In order to test the anti-disturbance ability of the control system, a load mutation experiment is designed. The experiment runs at a speed of 500 rpm and provides an instantaneous 1.5 N m moment to detect phase A current information. In order to enhance the accuracy of the system, we expanded the current information collected in this experiment. This is shown in Figs. 12, 13, and 14. Where red curve is the A-phase current and blue curve is the Q-axis current.

It can be seen from the experimental curve that during the load mutation of 1.5 N m, the anti-disturbance ability of LADRC is relatively weak. The specific data of current response time is shown in Table 4.

Conclusion

In light of the advantages and disadvantages of LADRC and NLADRC in practical engineering, SADRC is designed to enhance the control effect of PMSM by incorporating the strengths of both LADRC and NLADRC. Due to the functional characteristics of $fal_s(e, \alpha_i, \delta_1, \delta_2)$, SADRC can maintain good control effect when the error changes in a wide range. Through step experiments, steady-state experiments and load mutation experiments, the actual effects of the LADRC, NLADRC, and SADRC are compared, the experimental results verify the superiority of the SADRC.

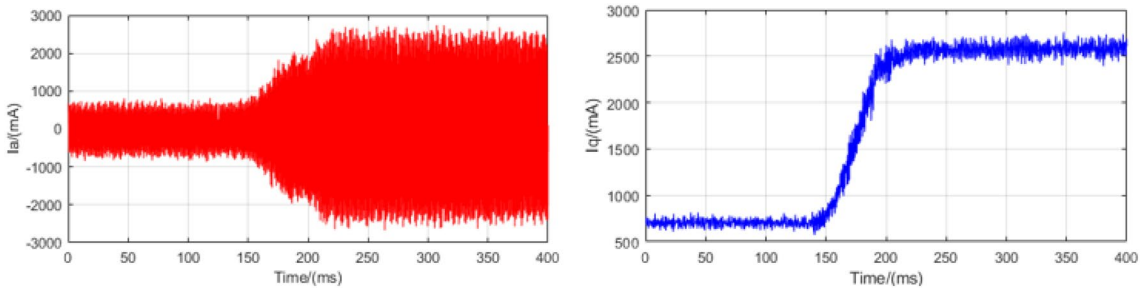

Figure 12. Load mutation experimental current plot based on LADRC.

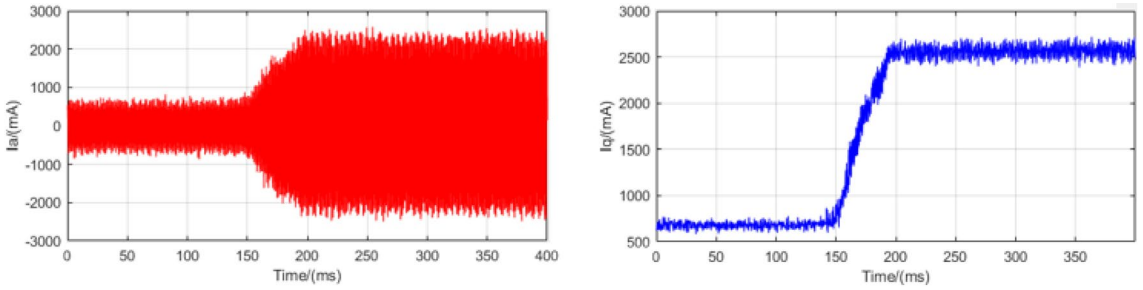

Figure 13. Load mutation experimental current plot based on NLADRC.

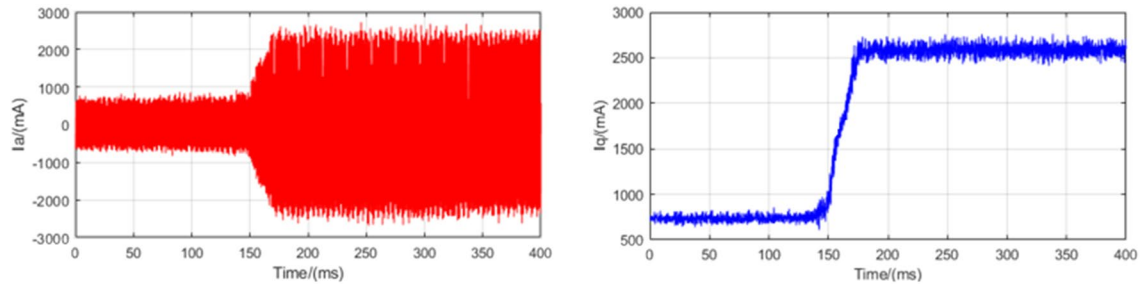

Figure 14. Load mutation experimental current plot based on SADRC.

	LADRC	NLADRC	SADRC
Δt(ms)	272	168	112

Table 4. Load mutation adjustment time.

Data availability

The datasets generated or analyzed during this study are available from the corresponding author on reasonable request.

Received: 17 May 2023; Accepted: 6 November 2023
Published online: 16 November 2023

References

1. Guo, B., Bacha, S. & Alamir, M. A review on ADRC based PMSM control designs. In *Proceedings of the IECON 2017—3rd Annual Conference of the IEEE Industrial Electronics Society, Beijing, China, 29 Oct–1 Nov 2017*. Vol. 3. 1747–1753 (2017).
2. Zhou, X., Sun, J., Li, H. & Song, X. High performance three-phase PMSM open-phase fault-tolerant method based on reference frame transformation. *IEEE Trans. Ind. Electron.* **66**(10), 7571–7580 (2019).
3. Yuan, X., Zhang, C. & Zhang, S. Torque ripple suppression for open-end winding permanent-magnet synchronous machine drives with predictive current control. *IEEE Trans. Ind. Electron.* **67**(3), 1771–1781 (2020).
4. Mansoor, A.K., Salih, T.A., & Abdullah, F. Speed control of separately excited D.C. motor using self-tuned parameters of PID controller. *Tikrit J. Eng. Sci.* (2022).

5. Ze, Q., Kou, P., Liang, D. & Liang, Z. Fault-tolerant performances of switched reluctance machine and doubly salient permanent magnet machine in starter/generator system. In *2014* 17th *International Conference on Electrical Machines and Systems (ICEMS)*. 3417–3423 (2014).
6. Nassim, M., & Abdelkader, A. *Speed Control of DC Motor Using Fuzzy PID Controller*. arXiv: abs/2108.05450 (2021).
7. Yang, J., Chen, W., Li, S., Guo, L. & Yan, Y. Disturbance/uncertainty estimation and attenuation techniques in PMSM drives—A survey. *IEEE Trans. Ind. Electron.* **64**(4), 3273–3285 (2017).
8. Luo, M. *et al.* Full-order adaptive sliding mode control with extended state observer for high-speed PMSM speed regulation. *Sci. Rep.* **13**, 6200 (2023).
9. Wang, S. *et al.* Sliding mode control with an adaptive switching power reaching law. *Sci. Rep.* **13**, 16155 (2023).
10. Wang, Y., Feng, Y., Zhang, X. & Liang, J. A new reaching law for antidisturbance sliding-mode control of pmsm speed regulation system. *IEEE Trans. Power Electron.* **35**(4), 4117–4126 (2020).
11. Gao, S. *et al.* Model-free hybrid parallel predictive speed control based on ultralocal model of PMSM for electric vehicles. *IEEE Trans. Ind. Electron.* **69**(10), 9739–9748 (2022).
12. Han, J. *Active Disturbance Rejection Control Technique: The Technique for Estimating and Compensating the Uncertainties* (National Defense Industry Press, 2008).
13. Gao, Z., Huang, Y. & Han, J. An alternative paradigm for control system design. In *Proceedings of the 40th IEEE Conference on Decision and Control, Orlando, FL, USA, 4–7 December 2001*. Vol. 5. 4578–4585 (2001).
14. Gao, Z. Scaling and bandwidth-parameterization based controller tuning. In *Proceedings of the American Control Conference*. Vol. 6. 4989–4996 (2003).
15. Zhang, P., Zhang, J., Du, X., Xia, H. & Wu, Y. Comparative study on LADRC and NLADRC of VGT-EGR system in diesel engine. In *2020 39th Chinese Control Conference (CCC), Shenyang, China*. 5566–5577. https://doi.org/10.23919/CCC50068.2020.9189010 (2020).
16. Li, J., Xia, Y., Qi, X. & Gao, Z. On the necessity, scheme, and basis of the linear-nonlinear switching in active disturbance rejection control. *IEEE Trans. Ind. Electron.* **64**, 1425–1435 (2017).
17. Li, M. *et al.* Active disturbance rejection position servo control of PMSLM based on reduced-order extended state observer. *Chin. J. Electric. Eng.* **6**(2), 30–41 (2020).
18. Li, J. *et al.* Absolute stability analysis of non-linear active disturbance rejection control for single-input-single-output systems via the circle criterion method. *IET Control Theory Appl.* **9**(15), 2320–2329 (2015).
19. Qi, X., Li, J., Xia, Y. & Gao, Z. On the robust stability of active disturbance rejection control for SISO systems. *Circuits Syst. Signal Process* https://doi.org/10.1007/s00034-016-0302-y (2016).
20. Zhao, Z. L. & Guo, B. Z. On convergence of the nonlinear active disturbance rejection control for MIMO systems. *Slam J. Control Optim.* **51**(2), 1727–1757 (2013).
21. Hao, Z. *et al.* Linear/nonlinear active disturbance rejection switching control for permanent magnet synchronous motors. *IEEE Trans. Power Electron.* **36**(8), 9334–9347. https://doi.org/10.1109/TPEL.2021.3055143 (2021).
22. Lin, P. *et al.* A class of linear–nonlinear switching active disturbance rejection speed and current controllers for PMSM. *IEEE Trans. Power Electron.* **36**, 14366–14382 (2021).

Author contributions

Methodology, Y.L.; validation, Y.L. and L.X.; experiment, Y.L. and X.C.; writing—original draft preparation, Y.L. and L.X.; writing—review and editing, Y.L., L.X. and X.L.; funding support, X.L., L.X. and X.T. All authors have read and agreed to the published version of the manuscript.

Competing interests

The authors declare no competing interests.

Additional information

Supplementary Information The online version contains supplementary material available at https://doi.org/10.1038/s41598-023-46881-8.

Correspondence and requests for materials should be addressed to L.X.

Reprints and permissions information is available at www.nature.com/reprints.

Publisher's note Springer Nature remains neutral with regard to jurisdictional claims in published maps and institutional affiliations.